DEVELOPMENT AND EXPERIMENTAL STUDY OF INFRARED BELT DRYER FOR RAPESEED
/
用于油菜籽干燥的红外带式干燥机研制和实验

Prof. Ph.D. Eng. Yang M.J.[1)], Ms. Stud. Eng. Liu B.[1)], Ms. Stud. Eng. Yang Z.R.[1)], Ms. Eng. Ding Z.Y.[1)], Prof. Ph.D. Eng. Yang L.[1)], Prof. Ph.D. Eng. Xie S.Y.[1)], Prof. Eng. Chen X.B.*[2)]

[1)] Southwest University, College of Engineering and Technology, Chongqing Key Laboratory of Agricultural Equipment for Hilly and Mountainous Regions / P. R. China;
[2)] Agricultural Machinery Quality Control and Inspection Technology Centre, Nanjing Research Institute for Agricultural Mechanization Ministry of Agriculture / P. R. China
Tel: 8613883002509; E-mail: ymingjin@swu.edu.cn

Keywords: *belt dryer, infrared drying, mathematic model, rapeseed, design and development*

ABSTRACT

According to matches of radiation properties of infrared heater and rapeseed, a small-scale infrared belt dryer was developed and its drying performance was tested and validated. Control factor of layer thickness has the highest significant level of impact on rapeseed effective moisture diffusivity and it is followed by factors of temperature, initial moisture content and radiation distance, sequentially. Two-term model gives the best fit to experimental data of moisture ratio, and it is followed by Page model. Both models are effective to predict moisture ratio of rapeseed infrared drying, with coefficient of correlation higher than 0.999.

摘要

基于红外加热元件辐射特点和油菜籽的匹配关系，开发了一套小型红外带式干燥机，并测试和验证了它的干燥性能。研究表明，料层厚度对油菜籽有效水分扩散系数影响最显著，其次是温度和初始含水率，辐射距离影响最小。Two-term 模型对水分比实验值的拟合度最好，Page 模型次之，两模型都具有很好的拟合效果，其相关系数均大于0.999。

INTRODUCTION

Rape (*Brassica campestris* L.) is planted for oil production, protein, forage, nectar and energy. Rapeseed is the third-leading source of vegetable oil and second-leading source of protein worldwide. China is a major country of rapeseed production and consumption, while the region of Yangtze River is the main rape planting area, rape (*Brassica napus* L.) as the main species, where harvest period often runs into rainy season of high temperature and high humidity. The freshly harvested rapeseed of high moisture content is susceptible to subject to deteriorations such as overheat, acidification and mildew, primarily due to its high-water activity *(Gao et al., 2016; Yang et al., 2012)*.

Artificial drying is required for the safe post-harvest process and storage of rapeseed. Solar drying, especially open sun drying and hot-air drying are still main options for rapeseed. Even though open sun drying offers low capital and operating costs and little expertise is required, its major disadvantages being extremely dependency on weather and large land areas needed for the shallow drying layer *(Aghbashlo et al., 2013)*. As for hot air drying, it involves product exposure to a continuous air flow to remove moisture, which leads to high energy demand *(Onwude et al., 2016)*. Compared to hot air drying, infrared radiation heating has many advantages such as greater energy efficiency, heat transfer rate and heat flux, which results in reduced drying time and higher drying rate *(Kayran et al., 2017)*. Infrared energy can be transferred from source to product surface directly without heating the surrounding air. However, when it falls on the other parts (such as tray) apart from product surface, they get heated, and as a result, the temperature of the surrounding increases, which helps reduce the moisture of the product *(Pawar et al., 2017)*.

Infrared drying is particularly suitable for thin layers of product with large surface exposed to radiation, and it has gained popularity as an alternative drying method for a variety of agricultural products *(Kayran et al., 2017)*. Infrared drying either alone or combined with others offers many advantages (such as greater energy efficiency, higher drying rate and better quality of dried product) over convective air drying under similar drying conditions. Because of a synergistic effect, the combination of infrared drying and hot

air drying has recently received much attention as novel thermal heat drying method, either to augment or completely replace the conventional drying method to improve overall process efficiency *(Onwude et al., 2016; Zhang et al., 2015)*.

Many studies have reported on the applications of infrared drying or combination with others such as strawberry *(Adak et al., 2017)*, red pepper *(Zhou et al. 2016)*, tomato *(Kocabiyik et al. 2016)*, bean seeds *(Doymaz, 2015)*, rice *(Okeyo et al., 2017)* and others. However, there is no information in the literature about infrared drying of rapeseed. The main objectives of this study were to develop a small-scale infrared belt dryer and investigate the effect of process parameters on the drying performance, fit the experimental data to 5 thin-layer drying models and compute effective moisture diffusivity of rapeseeds.

MATERIAL AND METHODS

DESIGN AND DEVELOPMENT OF THE DRYER

Overall Design

Considering physical properties of rapeseed and scale-up purpose of the infrared belt dryer, a small-scale infrared belt dryer was designed and developed, with dimensions of length 1.0 m, width 0.4 m, and height 0.6 m, as shown in Fig.1. The wet rapeseed is fed from feed port and flows onto the upper conveyer belt. There is a baffle plate in the feed port that acts as a cushion to the fall of the seed. The seed is delivered by conveyer belts in the upper and lower sections of the drying chamber sequentially, and in midway of the delivering, seed passes through a guide chute. During delivering, seed gets heated mainly by the infrared radiation, and the surrounding air is heated mainly by other heated parts in the drying chamber (such as belts, walls, etc.). The synergistic effect of infrared radiation and hot air benefits the moisture removal of the rapeseed. The delivery speed of the seed is controlled by a microcontroller based control system as required and the infrared radiation distance is adjustable by manipulating the thread screw.

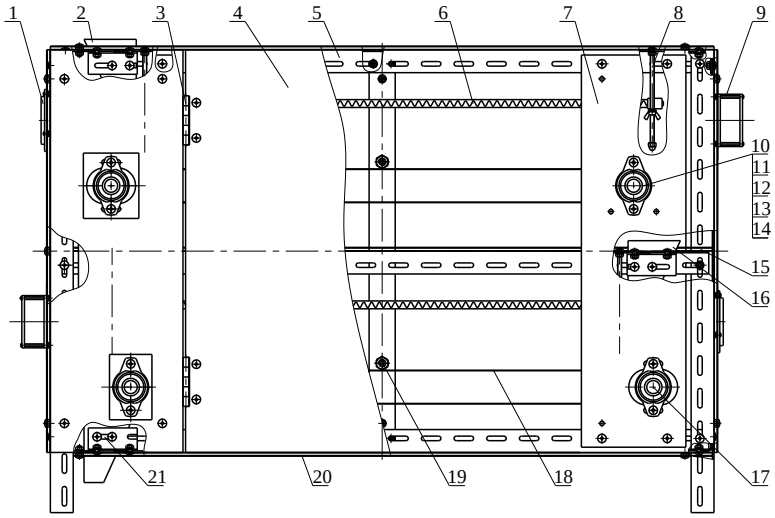

Fig. 1 - Structure diagram of the infrared belt dryer

1 – vent; 2 – feed port; 3 – hinge; 4 – opening; 5 – v-shaped steel; 6 – infrared heater; 7 – side plate; 8 – thread screw; 9 – axial flow fan; 10 – drive roller; 11 – bearing seat; 12 – coupling; 13 – stepping motor; 14 – motor bracket; 15 – baffle plate; 16 – guide chute; 17 – driven roller; 18 – conveyer belt; 19 – temperature sensor; 20 – wall; 21 – discharge port

Main Structure Design

Infrared heating system

Rapeseed is an unsaturated porous medium with sorptivity. According to matches of radiation properties of infrared heater and the product to be dried, since absorptivity of agricultural products at spectral range higher than 3 μm have their maximum absorptivity *(Pan et al., 2007)*, infrared heaters of wavelength of 3.3 μm were adopted for the radiation heating. Then, the surface temperature of the infrared heaters can be calculated as 878 K by the following expression (Wien's displacement law):

$$\lambda_{max} T = 2897.8, \ [\mu K] \quad (1)$$

where:

λ_{max} is wavelength of maximum emissivity, [μm];

T – absolute temperature, [K].

Radiation distance between infrared heater and the product affects drying efficiency and final quality of the dried product. The smaller the radiation distance is, the higher the radiant emittance will be, and the higher drying efficiency becomes, but the final quality of the dried product degrades. The irradiance of product can be calculated by the following expression *(Zhang et al., 2013)*:

$$M_e=H^2E_e, \text{ [W/m}^2\text{]} \quad (2)$$

where:

M_e is radiant emittance ("e" for "energetic"), [W/m^2];

H – radiation distance, [m];

E_e – irradiance at distance H, [W/m^2].

The radiant flux can be controlled by adjusting the radiation distance. According to pre-experiments, a range of radiation distance 50-100 mm was defined for the infrared belt dryer in this study.

The power (or radiant power, radiant flux) of each infrared heater can be calculated as 795 W by the following expression *(Wang, 2003)*:

$$P=E_eA, \text{ [W]} \quad (3)$$

where:

P is radiant power, [W];

A – area of irradiance at distance H, [m^2].

Irradiance 3000 kW/m^2 and area of irradiance 0.265 m^2 were defined in this study.

Conveying system

The conveying system of the infrared belt dryer comprises an upper chamber unit and a lower chamber unit (as shown in Fig. 2), and each unit is composed of conveyer belt, drive roller, driven roller, bearing seat, coupling, motor bracket, and stepping motor. The conveyer belt is made of polytetrafluoroethylene (Teflon®), with evenly distributed square holes of side size 1 mm. The conveyer belt is driven by the stepping motor. Then, the rapeseed on the conveyer belts moves forward, as shown by the arrows in Fig. 2.

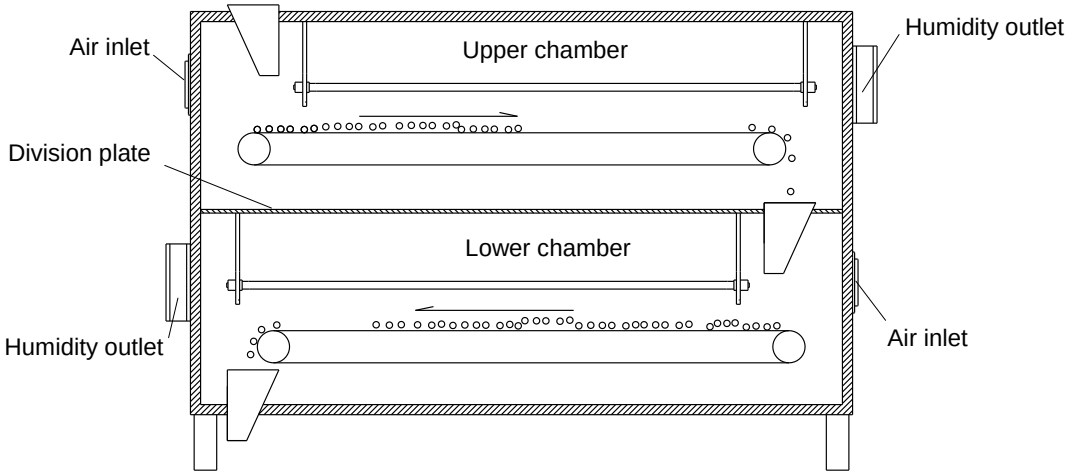

Fig. 2 - Conveying and ventilation diagram of the infrared belt dryer

Ventilation system

The ventilations in the upper chamber and lower chamber are separated by a division plate, as shown in Fig. 2. The axial flow fans 2B08038B12S (made by Asia Vital Components Co., Ltd) are installed at both humidity outlets, with parameters: operation voltage 12 V; maximum rotating speed 7000 r/min; maximum air flow rate 437 m^3/h. The air velocity and air flow rate can be controlled by means of frequency modulation. Moreover, there are evenly distributed holes on the conveyer belts which are beneficial to the ventilation in the drying chamber, especially in the thin layer product being processed.

Control System

The control system of the infrared belt dryer consists of modules of infrared heating, temperature sampling, motor control, ventilation, LCD display and keyboard input, and microcontroller STM32F407ZGT6 (made by STMicroelectronics) is the core platform of the system. Two temperature sensors WZP-187 PT100 (made by Shanghai Jiamin Instrument, Co. Ltd) are built at suitable positions above the product.

They sample the temperature information in the upper chamber and lower chamber individually. The feedback of temperature information is compared with pre-defined values and processed by the microcontroller. Then, based on the output of the process, the power of each infrared heater can be controlled (heating on/off) to obtain the pre-defined temperature in the drying chamber. The speed of the conveyer belts is driven by stepping motors and controlled by the motor control module. Since the speed of the conveyer belts is correlated to process time of the product in the drying chamber, the process time is controllable. Similarly, the air velocity and air flow rate in the drying chamber is controlled by the ventilation module.

RESULTS

PERFORMANCE STUDY OF THE DRYER

Experimental Procedures

The rapeseed (*Brassica napus* L.), Zhongzaliang 16, was harvested in Zhongxiang, Hubei Province, China. The impurities, cracked, germinated, mouldy seed and seed with green colour were manually removed so as to obtain uniform test samples. The initial moisture content (MC) of rapeseed was determined according to Chinese standard GB/T14489.1-2008 (China National standardizing committee, 2008). According to the initial MC 8.68 %d.b., test samples of the dry rapeseed were rewetted to MCs of 20 %d.b., 25 %d.b. or 30 %d.b. as required, by using the same method detailed in literature *(Gao et al., 2016)*.

Orthogonal Factorial Experiment Design technique based on Taguchi methodology was used to arrange experiments. Taking temperature, radiation distance, initial MC and layer thickness as control factors, and effective moisture diffusivity as evaluation index, levels of control factors were defined, as shown in Table 1. Experiments are designed in accordance with appropriate orthogonal array $L_9(3^4)$, a 3-level 4-factor array with 9 runs, and their arrangement is shown in Table 2.

Table 1

Levels of control factor

Level	Temperature *A*	Radiation distance *B*	Initial MC *C*	Layer thickness *D*
	[°C]	[mm]	[%d.b.]	[mm]
1	95	80	20	4
2	100	100	25	6
3	105	120	30	8

Table 2

Experiment arrangements and results of effective moisture diffusivity D_{eff}

No.	Factor A	Factor B	Factor C	Factor D	D_{eff} [10^{-9}m^2/s]
1	1	1	1	1	1.863
2	1	2	2	2	3.371
3	1	3	3	3	4.029
4	2	1	2	3	4.758
5	2	2	3	1	1.917
6	2	3	1	2	3.726
7	3	1	3	2	3.956
8	3	2	1	3	5.165
9	3	3	2	1	2.036

Effective moisture diffusivity can be calculated by the following expression (*Yang et al, 2014*):

$$\ln MR = \ln\frac{8}{\pi^2} - \frac{\pi^2 D_{eff} t}{L^2}, \text{ [dimensionless]} \quad (4)$$

where:

MR is moisture ratio, [dimensionless]; $MR=\left(M-M_e\right)/\left(M_i-M_e\right)$, *M* is the instantaneous MC, [%d.b.];

M_i is the initial MC, [%d.b.]; M_e is the equilibrium MC, [%d.b.];

D_{eff} – effective moisture diffusivity, [m^2/s];

t – drying time, [s];

L – layer thickness, [m].

For simplification, it was assumed that the surface of kernel remained dry throughout the drying process, then M_e=0 *(Thakor et al., 1999)*. Effective moisture diffusivity is typically determined by plotting experimental drying data in terms of ln*MR* versus drying time *t* in Equation (4), because the plot gives a straight line with a slope as follows: $\pi^2 D_{eff}/L^2$.

Drying Characteristics

The experimental moisture ratios of rapeseed versus drying time for different runs were plotted, as shown in Fig. 3. The drying characteristics curves of rapeseed under different combinations of drying conditions largely show a same tendency of change with drying time, namely, that moisture ratio exponentially decreases with drying time. No obvious constant rate drying stage is observed during the infrared drying of rapeseed, moisture removal is mainly processed during falling rate drying stage, and most of the moisture removal is finished in the first half stage. After drying of 30 min, the moisture ratios of all runs in Table 2 are less than 0.4 (the corresponding MCs are less than 9 %d.b.) which is a qualified MC level to safe storage of rapeseed in China.

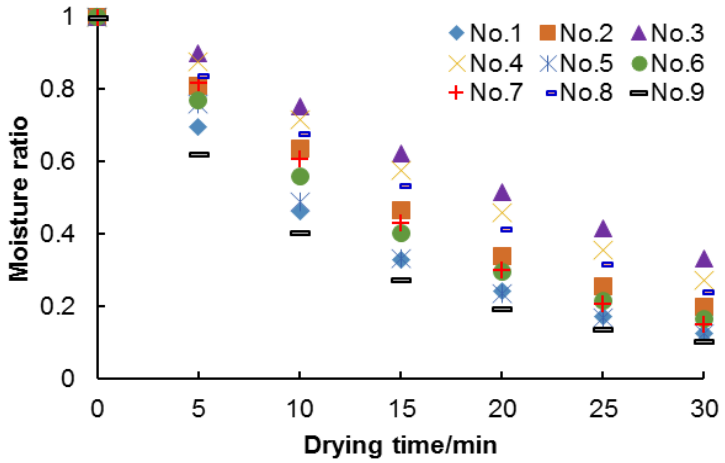

Fig. 3 - Experimental moisture ratios of rapeseed, for different runs

Statistical analyses of range and variance were performed to obtain the impacts and their significance of each control factor on the effective moisture diffusivity of rapeseed during infrared drying. Range analysis results were shown in Table 3, and variance analysis results were shown in Table 4. The values in cells of each level of the control factors in Table 3 represent mean diffusivities of the corresponding levels and factors. The delta values of each factor represent the biggest change of mean diffusivities of the factor, namely the impact level of each factor. The numbers in the rank row indicate the impact significance of the control factors. The reason why control factor of radiation distance of infrared heater has the lowest significance of impact on the effective moisture diffusivity can be explained as: even though radiation distance affects the irradiance of infrared heating, the on/off of the heater is controlled by temperature information, which determines the total radiant emittance.

Range analysis and variance analysis show that: the factor of layer thickness has the highest significant level of impact on rapeseed effective moisture diffusivity during infrared drying and it is followed by factors of temperature, initial MC and radiation distance, sequentially. The *F*-ratio of each control factor was compared to a critical value corresponding to a certain pre-selected probability, resulting in probabilities of 99.0 %, 83.6 %, and 51.6 % that control factors are in fact due to chance because of layer thickness, temperature, and initial MC, respectively. $A_3B_1C_1D_3$ and $A_1B_3C_3D_1$ are the optimal level combination and the worst level combination of the control factors that benefits to the effective moisture diffusivity, respectively.

According to optimal engineering average strategy *(Wang, 2004)*, the effective moisture diffusivities of any level combinations of the control factors can be calculated. The calculated diffusivities of combinations of $A_3B_1C_1D_3$ and $A_1B_3C_3D_1$ were obtained and compared with tested data, as shown in Table 5. Of which, the tested diffusivities of combinations of $A_3B_1C_1D_3$ and $A_1B_3C_3D_1$ were obtained by following the same experimental method aforementioned. As can be seen in Table 5, the optimal level combination, namely $A_3B_1C_1D_3$, shows better performance for moisture removal than any level combination in Table 2.

Table 3

Range analysis

Level	Factor A	Factor B	Factor C	Factor D
1	3.088	3.526	3.585	1.939
2	3.467	3.484	3.388	3.684
3	3.719	3.264	3.301	4.651
Delta	0.631	0.262	0.284	2.712
Rank	2	4	3	1

Table 4

Variance analysis

Source of variance	Degree of freedom	Sum of squares	Mean sum of squares	*F*-ratio	Critical *F*-ratio
Factor A	2	0.606	0.303	5.090	$F_{0.25}(2,2)=3.0$
Factor B	2	0.119	0.060	Error	$F_{0.10}(2,2)=9.0$
Factor C	2	0.127	0.063	1.066	$F_{0.01}(2,2)=99.0$
Factor D	2	11.336	5.668	95.224	/
Total	8	12.188	/	/	/

Table 5

Validation of effective moisture diffusivities

Combinations	Tested diffusivity	Calculated diffusivity	Relative error
	[10^{-9}m^2/s]	[10^{-9}m^2/s]	[%]
$A_3B_1C_1D_3$	5.586	5.206	6.80
$A_1B_3C_3D_1$	1.528	1.317	13.81

Mathematical Modelling

For further investigation of the drying performance, the experimental drying data of rapeseed moisture ratio under different conditions were fitted into 5 commonly used thin-layer drying models. The statistical results of the different models, including the drying model coefficients and the comparison criteria used to evaluate goodness of fit, namely, coefficient of correlation (R^2), reduced chi-square (χ^2) and root mean square error (*RMSE*), are listed in Table 6.

The coefficient of correlation, the reduced chi-square and the root mean square error can be calculated as follows:

$$R^2 = 1 - \frac{\sum_1^N \left(MR_{\exp,i} - MR_{\text{pre},i}\right)^2}{\sum_1^N \left(\overline{MR_{\exp}} - Mr_{\text{pre},i}\right)^2}, \text{[dimensionless]} \quad (5)$$

$$\chi^2 = \frac{\sum_1^N \left(MR_{\exp,i} - MR_{\text{pre},i}\right)^2}{N\text{-}n}, \text{[dimensionless]} \quad (6)$$

$$RMSE = \sqrt{\frac{\sum_1^N \left(MR_{\exp,i} - MR_{\text{pre},i}\right)^2}{N}}, \text{[dimensionless]} \quad (7)$$

where:

$MR_{exp,i}$ is the *i*th experimental moisture ratio, and $MR_{pre,i}$ is the *i*th predicted moisture ratio;

N – the number of observation;

n – the number of constants in the mathematical model.

Table 6

Statistical results obtained from different models

Model	Parameter									Mean value
	Run 1	Run 2	Run 3	Run 4	Run 5	Run 6	Run 7	Run 8	Run 9	
1 Newton: $MR=\exp(-kt)$										
k	0.073	0.051	0.033	0.039	0.070	0.060	0.057	0.043	0.086	/
R^2	0.9986	0.9924	0.9808	0.9816	0.9940	0.9980	0.9834	0.9911	0.9961	0.9907
χ^2	0.000146	0.000612	0.000994	0.001131	0.000599	0.000178	0.001448	0.000613	0.000437	0.000684
RMSE	0.0112	0.0229	0.0292	0.0311	0.0227	0.0124	0.0352	0.0229	0.0194	0.0230
2 Page: $MR=\exp(-kt^n)$										
k	0.082	0.033	0.016	0.018	0.054	0.049	0.028	0.026	0.118	/
n	0.957	1.158	1.254	1.254	1.097	1.070	1.251	1.177	0.878	/
R^2	0.9991	0.9993	0.9996	0.9999	0.9966	0.9994	0.9995	1.0000	0.9998	0.9992
χ^2	0.000114	0.000074	0.000029	0.000011	0.000433	0.000067	0.000058	0.000002	0.000028	0.000091
RMSE	0.0090	0.0073	0.0046	0.0028	0.0176	0.0069	0.0064	0.0012	0.0045	0.0067
3 Henderson and Pabis: $MR=a\exp(-kt)$										
a	0.996	1.025	1.036	1.037	1.020	1.013	1.039	1.026	0.983	/
k	0.073	0.053	0.035	0.041	0.071	0.061	0.059	0.045	0.084	/
R^2	0.9986	0.9947	0.9890	0.9888	0.9952	0.9985	0.9888	0.9940	0.9965	0.9938
χ^2	0.000170	0.000555	0.000784	0.000940	0.000614	0.000165	0.001309	0.000536	0.000457	0.000614
RMSE	0.0110	0.0199	0.0237	0.0259	0.0209	0.0109	0.0306	0.0196	0.0181	0.0201
4 Logarithmic: $MR=a\exp(-kt)+c$										
a	0.962	1.176	1.946	1.700	1.035	1.044	1.260	1.345	0.934	/
k	0.080	0.040	0.015	0.019	0.069	0.057	0.041	0.028	0.100	/
c	0.041	-0.165	-0.932	-0.687	-0.018	-0.035	-0.241	-0.338	0.063	/
R^2	0.9995	0.9976	0.9976	0.9981	0.9953	0.9988	0.9960	0.9993	0.9998	0.9980
χ^2	0.000083	0.000315	0.000223	0.000205	0.000749	0.000168	0.000614	0.000085	0.000034	0.000275
RMSE	0.0069	0.0134	0.0113	0.0108	0.0207	0.0098	0.0187	0.0070	0.0044	0.0114
5 Two-term: $MR=a\exp(-k_0t)+b\exp(-k_1t)$										
a	0.028	1.171	1.186	1.351	1.101	1.055	1.302	1.655	0.458	/
k_0	-0.010	0.060	0.042	0.053	0.077	0.063	0.073	0.061	0.053	/
b	0.975	-0.171	-0.186	-0.350	-0.101	-0.055	-0.302	-0.655	0.542	/
k_1	0.079	0.244	0.211	0.151	6.558	6.184	0.254	0.108	0.139	/
R^2	0.9995	0.9995	0.9998	0.9999	0.9983	0.9998	0.9999	1.0000	1.0000	0.9996
χ^2	0.000107	0.000110	0.000022	0.000020	0.000361	0.000034	0.000015	0.000000	0.000001	0.000074
RMSE	0.0068	0.0069	0.0031	0.0030	0.0124	0.0038	0.0025	0.0001	0.0006	0.0044

Notes: k, k_0, k_1, n, a, b and c are model constants.

In this study, the nonlinear regression analysis was performed with statistical software, SPSS16.0. The higher the R^2 values and the lower the χ^2 and *RMSE* values, the better the goodness of fit *(Wang et al., 2007)*. As it can be seen in Table 6, the Two-term model gives the best fit to experimental data of moisture ratio, with R^2 0.9996, χ^2 0.000074 and *RMSE* 0.0044; it is followed by the Page model, with R^2 0.9992, χ^2 0.000091 and *RMSE* 0.0067.

Experimental moisture ratio values of the optimal level combination, namely $A_3B_1C_1D_3$, were employed to validate the effectiveness of the Two-term model and Page model. The predicted moisture ratio values of these two models were compared with experimental values, as shown in Fig. 4. The Two-term model and Page model both fit very well the experimental data: R^2 0.9996, χ^2 0.00067 and *RMSE* 0.0054 for the former model and R^2 0.9993, χ^2 0.000072 and *RMSE* 0.0072 for the latter model. However, to simplify the mathematical model, the convenience for process control and optimization of drying technology, the Page model is preferred to the rapeseed infrared drying.

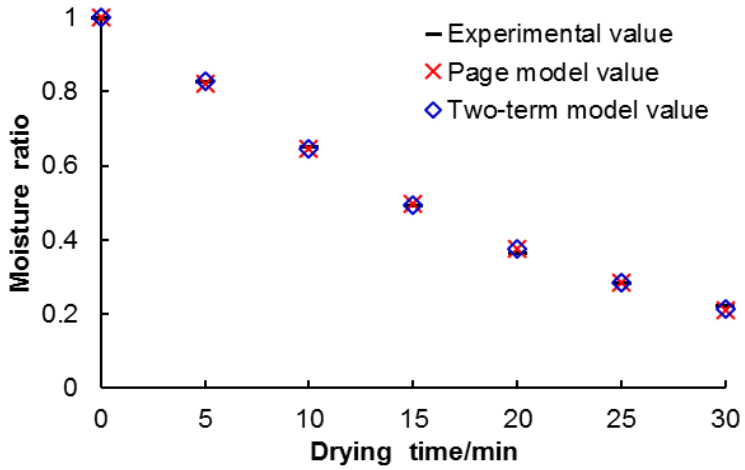

Fig. 4 - Validation of mathematical models

Continuous Drying Experiment

According to the optimal level combination ($A_3B_1C_1D_3$) of drying parameters, namely temperature 105 ^oC, radiation distance 80 mm, initial MC 20%d.b. and layer thickness 8 mm, rapeseed of 1.109 kg was loaded into the infrared belt dryer for continuous drying experiments (as shown in Fig. 5). The drying time was set as 30 min via keyboard input, and all the drying operations were controlled by the control system of the infrared belt dryer. The experimental results show that the mass of the dried rapeseed was 0.967 kg, namely its MC was 4.63%d.b. which is much less than the qualified MC level to safe storage of rapeseed in China.

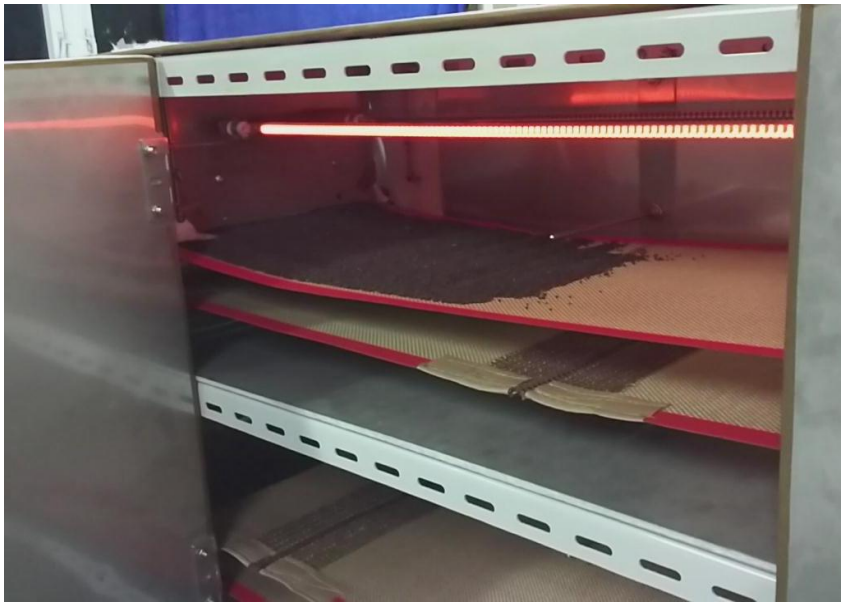

Fig. 5 - Continuous drying experiment

CONCLUSIONS

According to matches of radiation properties of infrared heater and rapeseed, a small-scale infrared belt dryer was developed. The effect of process parameters on the drying performance of rapeseed was investigated, the goodness of fit of selected mathematical models for infrared drying was evaluated, and the continuous drying experiment was conducted. The main conclusions are as follows:

- during rapeseed infrared drying, no obvious constant rate drying stage is observed, moisture removal is mainly processed during falling rate drying stage, and rapeseed moisture ratio exponentially decreases with drying time.
- control factor of layer thickness has the highest significant level of impact on rapeseed effective moisture diffusivity during infrared drying, and it is followed by factors of temperature, initial MC and radiation distance, sequentially.
- Two-term model gives the best fit to experimental data of moisture ratio, with coefficient of correlation 0.9996, reduced chi-square 0.000074 and RMSE 0.0044; it is followed by the Page model, with coefficient of correlation 0.9992, reduced chi-square 0.000091 and RMSE 0.0067, which shows that both models are effective to predict the moisture ratio of rapeseed infrared drying.
- To simplify the mathematical model, the convenience for process control and optimization of the drying technology, the Page model is preferred to rapeseed infrared drying.

ACKNOWLEDGEMENTS

The study has been funded by the National Natural Science Foundation of China (No. 31301575), Ph.D. Research Project of Southwest University (No. SWU115011), and Fund from Key Laboratory of Modern Agricultural Equipment, Ministry of Agriculture, China (No. 201601001).

REFERENCES

[1] Adak N., Heybeli N. and Ertekin C., (2017), Infrared drying of strawberry, *Food Chemistry*, vol. 219, pp. 109-116, Ed. Elsevier, London/U.K.;

[2] Aghbashlo M., Mobli H., Rafiee S. and Madadlou A., (2013), A review on exergy analysis of drying processes and systems, *Renewable & Sustainable Energy Reviews*, vol. 22, pp. 1-22, Ed. Elsevier, London/U.K.;

[3] Doymaz I., (2015), Infrared drying characteristics of bean seeds, *Journal of Food Processing and Preservation*, vol. 39, issue 6, pp. 933-939, Ed. Wiley, Malden/U.S.A.;

[4] Gao B., Guo M.B., Yang L., Wu D.K. and Yang M.J., (2016), Heat and mass transfer during hot-air drying of rapeseed: CFD approach and evaluation, *INMATEH Agricultural Engineering Journal*, vol. 50, issue 3, pp. 73-82, Ed. INMA Bucharest, Bucharest/Romania;

[5] Kayran S., and Doymaz I., (2017), Infrared drying and effective moisture diffusivity of apricot halves: influence of pre-treatment and infrared power, *Journal of Food Processing and Preservation*, vol. 41, issue 2, pp. 1-8, Ed. Wiley, Malden/U.S.A.;

[6] Kocabiyik H., Yilmaz N., Tuncel N.B., Sumer S.K., and Buyukcan M.B., (2016), Quality properties, mass transfer characteristics and energy consumption during shortwave infrared radiation drying of tomato, *Quality Assurance and Safety of Crops & Foods*, vol. 8, issue 3, pp. 447-456, Ed. Wageningen Academic Publishers, Wageningen/Netherlands;

[7] Okeyo A., Olatunde G., Atungulu G., Sadaka S., and Mckay T., (2017), Infrared drying characteristics of long-grain hybrid, long-grain pureline, and medium-grain rice cultivars, *Cereal Chemistry*, vol. 94, issue 2, pp. 251-261, Ed. AACC International, St Paul/U.S.A.;

[8] Onwude D.I., Hashim N., and Chen G.N., (2016), Recent advances of novel thermal combined hot air drying of agricultural crops, *Trends in Food Science & Technology*, vol. 57, pp. 132-145;

[9] Pan Y.K., Wang X.Z., and Liu X.D., (2007), *Modern drying technology (现代干燥技术)*, ISBN 978-7-5025-9361-2, Chemical Industry Press, Beijing/P.R.C.;

[10] Pawar S.B. and Pratape V.M., (2017), Fundamentals of infrared heating and its application in drying of food materials: a review, *Journal of Food Process Engineering*, vol. 40, issue 1, pp. 1-15, Ed. Wiley, Malden/U.S.A.;

[11] Thakor N.J., Sokhansanj S., Sosulski F.W., and Yannacopoulos S., (1999), Mass and dimensional changes of single canola kernels during drying, *Journal of Food Engineering*, vol. 40, pp. 153-160, Ed. Elsevier, London/U.K.;

[12] Wang W.Z., (2004). *Design of experiments and analysis (试验设计与分析)*. Higher Education Press, Beijing/P.R.C.;
[13] Wang X.B., (2003), *Theoretical analysis and experimental study on combined convective and infrared radiation drying (红外辐射与对流联合干燥的理论分析及试验研究)*, PhD dissertation, China Agricultural University, Beijing/P.R.C.;
[14] Wang Z.F., Sun J.H., Liao X.J., Chen F., Zhao G.H., Xu J.H., and Hu X.S., (2007), Mathematical modelling on hot air drying of thin layer apple pomace, *Food Research International*, vol. 40, pp. 39-46, Ed. Elsevier Science Bv, Amsterdam/Netherlands;
[15] Yang G., He S., and Ding C., (2013), Study of the rapeseeds' quality storage after hot-air drying (油菜籽热风干燥后储藏品质的研究), *Journal of the Chinese Cereal and Oils Association*. vol. 28, issue 9, pp. 97-102, Ed. Chinese Cereal and Oils Association, Beijing/P.R.C.;
[16] Zhang M., Chen H.Z., Mujumdar A.S., Zhong Q.F., and Sun J.C., (2015), Recent developments in high-quality drying with energy-saving characteristic for fresh foods, *Drying Technology*, vol. 33, issue 13, pp. 1590-1600, Ed. Taylor & Francis Inc., Philadelphia/U.S.A.;
[17] Zhang Q.Q., Wen H.X., and Yuan Y.J., (2013), Research and design far infrared with drying equipment in vacuum (远红外联合低温真空干燥设备研究与设计), *Food & Machinery*, vol. 29, issue 1, pp. 157-160, Ed. Changsha University of Science and Technology, Changsha/P.R.C.;
[18] Zhou L.Y., Cao Z.Z., Bi J.F., Yi J.Y., Chen Q.Q., Wu, X.Y., and Zhou M., (2016), Degradation kinetics of total phenolic compounds, capsaicinoids and antioxidant activity in red pepper during hot air and infrared drying process, *International Journal of Food Science & Technology*, vol. 51, issue 4, pp. 842-853, Ed. Wiley, Hoboken/U.S.A.;
[19] *** China National standardizing committee, (2008), *Oilseeds - Determination of moisture and volatile matter content, GB/T14489.1-2008 (油料 水分及挥发物含量测定, GB/T14489.1-2008)*, Chinese Standard Press, Beijing/P.R.C.